



## Comparison of Segmentation Analysis in Nucleus Detection with GLCM Features using Otsu and Polynomial Methods

Dwiza Riana<sup>1</sup>, Jufriadif Na'am<sup>2</sup>, Daniati Uki Eka Saputri<sup>3\*</sup>, Sri Hadiani<sup>4</sup>, Faruq Aziz<sup>5</sup>, Suryadi Putra Liawatimena<sup>6</sup>, Alya Shafra Hewiz<sup>7</sup>, Dika Putri Metalica<sup>8</sup>, Teguh Herwanto<sup>9</sup>

<sup>1,2,8,9</sup>Computer Science, Faculty of Information Technology, Universitas Nusa Mandiri, Jakarta, Indonesia

<sup>3,5</sup>Information Systems, Faculty of Information Technology, Universitas Nusa Mandiri, Jakarta, Indonesia

<sup>4</sup>Informatics, Faculty of Information Technology, Universitas Nusa Mandiri, Jakarta, Indonesia

<sup>6</sup>Computer Science, BINUS Graduate Program – Doctor of Computer Science, Bina Nusantara University, Jakarta, Indonesia

<sup>7</sup>Faculty of Medicine, Universitas Airlangga, Surabaya, Indonesia

<sup>1</sup>dwiza@nusamandiri.ac.id, <sup>2</sup>jufriadifnaam@gmail.com, <sup>3</sup>daniati.due@nusamandiri.ac.id, <sup>4</sup>sri.shv@nusamandiri.ac.id,

<sup>5</sup>faruq.fqs@nusamandiri.ac.id, <sup>6</sup>suryadi@binus.edu, <sup>7</sup>hewizalya@gmail.com, <sup>8</sup>14220003@nusamandiri.ac.id,

<sup>9</sup>14220001@nusamandiri.ac.id

### Abstract

*Pap smear is a digital image generated from the recording of cervical cancer cell preparation. Images generated are susceptible to errors due to the relatively small cell sizes and overlapping cell nuclei. Therefore, accurate Pap smear image analysis is essential to obtain the right information. This research compares nucleus segmentation and detection using Grey Level Co-occurrence Matrix (GLCM) features in two methods: Otsu and Polynomial. The tested data consisted of 400 images sourced from RepoMedUNM, a publicly accessible repository containing 2,346 images. Both methods were compared and evaluated to obtain the most accurate features. The research results showed that the average distance of the Otsu method was 6.6457, which was superior to the Polynomial method with a value of 6.6215. Distance refers to the distance between the nucleus detected by the Otsu and the Polynomial method. Distance is an important measure to assess how closely the detection results align with the actual nucleus positions. It indicates that the Polynomial method produces nucleus detections that are on average closer to the actual nucleus positions compared to the Otsu method. Consequently, this research can serve as a reference for further studies in developing new methods to enhance the accuracy of identification.*

*Keywords: pap smear; cervical cancer; nucleus; GLCM otsu; GLCM polynomial*

### 1. Introduction

Pap smear analysis is crucial for the early detection of cervical cancer [1], [2], [3]. This analysis is highly necessary to provide accurate and comprehensive information about a patient's cervical cancer for diagnosis and to offer more treatment insights to doctors [4]. Inaccurate information can have a significant impact on misdiagnosis, which can lead to serious consequences [5].

Pap smear images represent cells from the cervix that have been prepared, stained, and analyzed under a microscope [6]. These images can provide insights into the condition of each cell [7], but they tend to be challenging and susceptible to errors [8]. The primary source of error is the relatively small cell sizes and overlapping cell nuclei [9], making them challenging to identify [10], [11]. Therefore, image analysis is

required in the image processing to assist in inspections and achieve more accurate results.

The accuracy level in image processing still needs improvement, especially for certain cell classes [12], [13], and most methods only perform very well on one or a few images [14]. This accuracy can be enhanced by comparing various parameters used in image processing, thereby allowing for better identification of cervical cancer.

Cervical cancer is the most common and highly feared cancer among women worldwide [15]. Cervical cancer arises from the development of abnormal cells [16], [17]. Each normal cell typically has a single nucleus [18], [19] that regulates cell activities. Cells with double or overlapping nuclei are indicative of cancerous cells [20], causing them to malfunction [21]. Given the position of these cells surrounded by other tissues with relatively thin cell sizes [22], there is a need for

segmentation development by comparing various techniques to improve accuracy.

Segmentation in separating objects in Pap smear images involves different attributes and features [23]. Images resulting from the recording of preparations under a microscope often exhibit poor contrast, neutrophils, overlapping cells, and uneven staining [24]. As a result, cells may appear to have more than one nucleus, as illustrated in Figure 1.

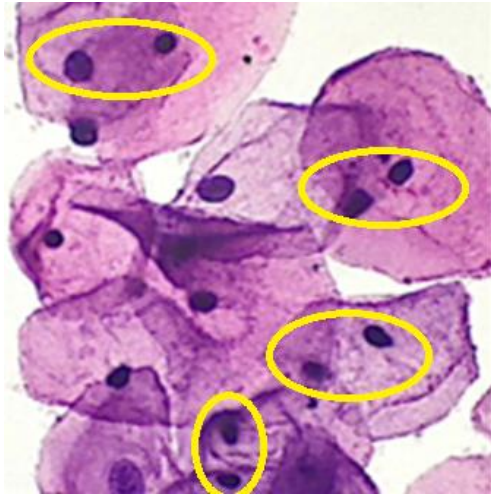


Figure 1. Appearance of cells with more than one nucleus.

Figure 1 presents cells containing more than one nucleus due to artifact interference, neutrophils, overlapping cells, and false edges [25], [26], thus, segmentation and detection of single nuclei in Pap

smear images require a reliable method. The Grey Level Co-occurrence Matrix (GLCM) technique is a method used to analyze the spatial relationships between pixels in images [27]. In a study about nucleus detection in Pap smear images using a polynomial method to enhance image quality, thus facilitating the process of Pap smear cell image segmentation [33]. Another research proposed a segmentation method for the cytoplasmic area in Pap smear images that utilizes GLCM features [34]. This method is effectively used in various image applications and holds great potential in object detection in medical images. This research develops GLCM features in comparing the results of single nucleus analysis with Otsu and Polynomial methods. The analysis is supported by the application of Region of Interest (ROI) segmentation to compare the performance of both methods. The methods are trained with a detection model using the YOLO version 5 (You Only Look Once) deep learning algorithm to detect objects. As a result, the development yields two different image processing methods, namely GLCM Otsu and GLCM Polynomial, to support the detection of single cells in Pap Smear. GLCM Otsu and polynomial are utilized in thresholding processing and texture analysis.

## 2. Research Methods

Figure 2 illustrates the data recording flow used to obtain the test images in this research.

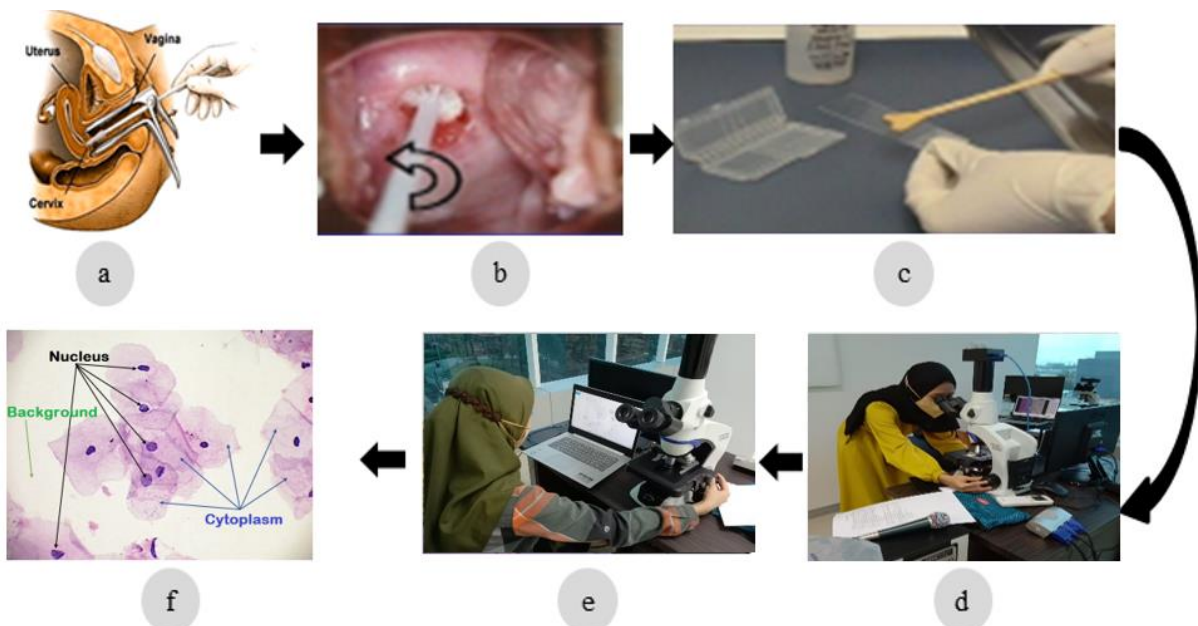


Figure 2. The process of collecting Pap smear images.

The process of obtaining Pap smear images from cervical cancer patients involves taking a sample by inserting a speculum into the patient's vagina (Figure

2.a). Within the speculum, there is a cytobrush used to collect fluid by rotating it (Figure 2.b). The fluid from the cytobrush is then placed on a prepared slide that has

been coated with preservCyt fluid (Figure 2.c). This preparation is placed under the Olympus CX33RTFS2 microscope and the X52-107BN microscope for observation (Figure 2.d). The observation results are recorded digitally using a computer with a Logitech HD webcam C525 camera (Figure 2.e), resulting in Pap smear images with a 40x magnification. The image format used is Joint Photographic Experts Group (JPG) with a size of 512 x 512 pixels. The resulting images exhibit cell overlap (Figure 2.f). The images are examined by combining the GLCM Otsu and GLCM Polynomial methods for single-cell nucleus detection in Pap smear. The research stages conducted are presented in Figure 3.

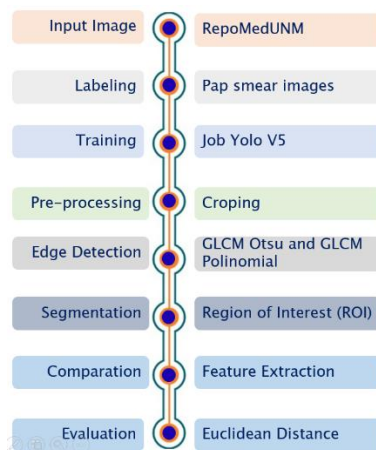


Figure 3. Stages of Research Methods

GLCM is a method for extracting texture features. GLCM measures the level of grayness between two pixels separated by a distance  $d$  and an angle  $\theta$ . The commonly used angles include 0 degrees, 45 degrees, 90 degrees, and 135 degrees [30]. Some of the generated features are:

Contrast represents the difference in color or grayscale levels in an image. The contrast value becomes 0 when adjacent pixels have identical values. The determination of the contrast value can be calculated using Formula 1.

$$\sum_i \sum_j (i - j)^2 p(i, j) \quad (1)$$

$i$  is the Rows,  $j$  is the Columns,  $p$  are the Rows and columns appear.

Correlation is the linear relationship of grayscale levels within an image, ranging from -1 to 1. The calculation of the correlation value is performed using Formula 2.

$$\sum_i \sum_j \frac{(i - \mu_i)(j - \mu_j)p(i, j)}{\sigma_i \sigma_j} \quad (2)$$

$\mu_i$  is the Rows average,  $\mu_j$  is the Column average,  $\delta_i$  is the sigma Row,  $\delta_j$  is the sigma Column.

Energy indicates the level of uniformity in an image. The higher the image uniformity, the higher the Energy

value. The calculation of the Energy value is performed using Formula 3.

$$\sum_i \sum_j p(i, j)^2 \quad (3)$$

$i$  are the Rows,  $j$  are the Columns,  $p$  is the Appearance of rows and columns.

Homogeneity describes the level of uniformity in an image. When all pixels in an image have uniform values, its homogeneity will be high. The calculation of the homogeneity value is performed using Formula 4.

$$\sum_i \sum_j \frac{p(i, j)}{1 + |i - j|} \quad (4)$$

$i$  are the Rows,  $j$  are the Columns,  $p$  = appearance of rows and columns

The Otsu method is one of the segmentation techniques that is similar to converting to grayscale images but simpler because it is easier to determine the threshold values for pixels. The Otsu method employs discriminant analysis to identify variables that function to separate the two visible sides [31]. The formula for finding the pixels can be seen in Formula 5.

$$p(i) = \frac{n_i}{N}, P(i) \geq 0, \sum_i^{256} p(i) = 1 \quad (5)$$

Then, to calculate the averages of both classes, you can refer to Formula 6 and 7.

$$m_1(t) = \sum_{t=1}^t i \cdot p(i) / w_1(t) \quad (6)$$

$$m_2(t) = \sum_{t=1}^t i \cdot p(i) / w_2(t) \quad (7)$$

The potential total sum of both classes, as stated in Formula 8, is equivalent to 1.

$$w_1(t) + w_2(t) = 1 \quad (8)$$

Thus, it can be concluded that Otsu can be considered as the between-class variance (BCV) as defined in Formula 9.

$$\delta_b^2(t) = w_1 \cdot [m_1(t) - m_T]^2 + w_2 \cdot [m_2(t) - m_T]^2 \quad (9)$$

The optimal value in Otsu thresholding is the maximum value of the between-class variance (BCV) as defined in Formula 10.

$$\max\{\delta_b^2(t)\} \quad (10)$$

The polynomial method in this research is used to enhance Pap smear images by performing contrast transformation and color enhancement [32].

Generally, the form of a polynomial equation of order  $r$  follows a formula similar to Formula 11.

$$y = a_0 + a_1x + a_2x^2 + \dots + arx^r \quad (11)$$

The polynomial technique has been utilized in previous research for the purpose of enhancing the quality of Pap smear images, particularly the RGB images within the image [33].

The purpose of transforming the image into a polynomial is to generate a highly significant color difference (contrast), enabling segmentation of the nucleus to be carried out [33].

The research was conducted on the RepoMedUNM dataset, which contains Pap smear images. RepoMedUNM offers 2,346 Thinprep type images and 3,793 non-Thinprep-type images [28]. The dataset used in this study consists of 400 images, comprising four types of cells: L-Sil, H-Sil, Koilocyt, and Parabasal cells.

The process continues with image labeling, which involves assigning class labels to each image. The

labeling process is carried out using Huawei technology [29]. The outcome of this process creates a labeled dataset that will be used to train the detection model. Labeled images are utilized to build the YOLO (You Only Look Once) version 5 model. During the training phase, the YOLO model can learn features and patterns related to classes in Pap smear images. This process yields network objects in the form of weights and biases.

Figure 4 is an implementation YOLOv5 for Pap smear detection involves utilizing RGB 3-channel input photos that are scaled to dimensions of 416x416 [35].

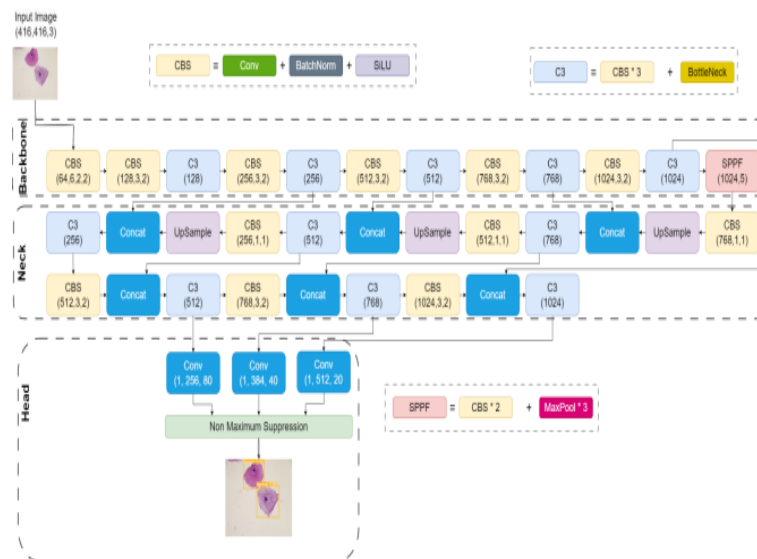


Figure 4. Image Detection Process with YOLO

The YOLOv5 model is employed, utilizing a backbone architecture that incorporates several Convolutional and C3 (Convolutional 3x3) layers to extract features from the images. The predictions are made using the YOLOv5 head, which comprises Convolutional, up sample, and Concatenation layers, utilizing the feature extraction outcomes obtained from different layers in the backbone. The ultimate forecasts for object detection, encompassing Pap smear detection, are derived from the Detect layer, which amalgamates outcomes from various layers within the model.

The image pre-processing is used to separate single cells, namely the cytoplasm from the nucleus. This stage involves cropping with the aim of efficiency and speeding up the process of forming single-cell images with only one nucleus.

The image that contains one nucleus is continued with the detection process using the Otsu and Polynomial methods. This process aims at different image processing by reducing the contrast of the original image.

The next step is segmentation to identify Regions of Interest (ROI). ROI includes selecting the largest single-cell nucleus. This process is used to locate areas containing countable objects and analyze them in more detail. This stage is focused on the relevant areas to reduce the overall analysis complexity. To compare the performance of the Otsu and Polynomial methods, feature extraction was carried out. This process yielded four GLCM features: contrast, correlation, energy, and homogeneity, each with its respective values.

The proximity between the GLCM features of Otsu and Polynomial methods was calculated using Euclidean distance with a reference GLCM feature. The results of this proximity calculation serve as the basis for evaluation to determine if the closeness of the two methods can produce a better accuracy in detecting nuclei in Pap smear images.

### 3. Results and Discussions

The input image presented in this article is one of the input images presented in Figure 5.

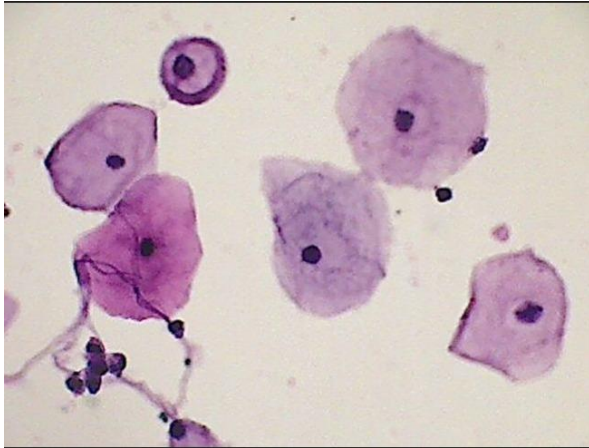


Figure 5. Input Image

The input image is the original image and xml file (class and bounding box) from Huawei's YOLO detection and classification output. Yolo classification data is presented in Figure 6.

Name	Size	Packed	Type	Modified	CRC32
K-CV 1904662-140022 (11).xml	1.698	400	Microsoft Edge HT...	18/10/2022 13:12	7976F4C2
K-CV 1904662-140022 (11).jpg	40.709		JPG File	26/08/2022 10:44	102D96888
K-CV 1904662-140022 (10).xml	2.373	445	Microsoft Edge HT...	18/10/2022 13:12	14A88A12A
K-CV 1904662-140022 (10).jpg	37.104	37.104	JPG File	26/08/2022 10:44	CC89FF9
K-CV 1904662-140020 (9).xml	2.018	419	Microsoft Edge HT...	18/10/2022 13:12	4498E169
K-CV 1904662-140020 (9).jpg	9.476	9.464	JPG File	26/08/2022 10:44	0D4F1E51
K-CV 1904662-140020 (8).xml	1.359	385	Microsoft Edge HT...	18/10/2022 13:12	334D30C0
K-CV 1904662-140020 (8).jpg	8.505	8.500	JPG File	26/08/2022 10:44	E315F8A3
K-CV 1904662-140015 (8).xml	3.364	481	Microsoft Edge HT...	18/10/2022 13:12	94441432
K-CV 1904662-140015 (8).jpg	13.567	13.555	JPG File	26/08/2022 10:44	43E4A402
K-CV 1904662-140015 (7).xml	2.022	426	Microsoft Edge HT...	18/10/2022 13:12	81B5818A
K-CV 1904662-140015 (7).jpg	9.035	9.027	JPG File	26/08/2022 10:44	A2189509
K-CV 1904662-140013 (7).xml	3.365	470	Microsoft Edge HT...	18/10/2022 13:12	3A5C656A
K-CV 1904662-140013 (7).jpg	12.797	12.788	JPG File	26/08/2022 10:44	D861905F
K-CV 1904662-140013 (6).xml	1.693	416	Microsoft Edge HT...	18/10/2022 13:12	CB131F4
K-CV 1904662-140013 (6).jpg	10.528	10.528	JPG File	26/08/2022 10:44	C71913FA
K-CV 1904662-140013 (5).xml	2.697	464	Microsoft Edge HT...	18/10/2022 13:12	1E17F189
K-CV 1904662-140009 (5).jpg	12.580	12.563	JPG File	26/08/2022 10:44	F4C3AD97
K-CV 1904662-140009 (4).xml	5.379	562	Microsoft Edge HT...	18/10/2022 13:12	7C81104D
K-CV 1904662-140009 (4).jpg	18.421	18.421	JPG File	26/08/2022 10:44	5CAC11F1
K-CV 1904662-140009 (3).xml	4.017	505	Microsoft Edge HT...	18/10/2022 13:12	E4D49F4D
K-CV 1904662-140009 (3).jpg	16.913	16.913	JPG File	26/08/2022 10:44	3F6C2A68
K-CV 1904662-140007 (4).xml	3.033	466	Microsoft Edge HT...	18/10/2022 13:12	84C9069F
K-CV 1904662-140007 (4).jpg	14.265	14.277	JPG File	26/08/2022 10:44	886C7821
K-CV 1904662-140005 (3).xml	3.701	491	Microsoft Edge HT...	18/10/2022 13:12	7832D05E
K-CV 1904662-140005 (3).jpg	14.234	14.234	JPG File	26/08/2022 10:44	94977F48
K-CV 1904662-140005 (2).xml	2.365	430	Microsoft Edge HT...	18/10/2022 13:12	0972C8B1
K-CV 1904662-140005 (2).jpg	15.545	15.523	JPG File	26/08/2022 10:44	R020282A

Figure 6. Original Image and XML File

The input image is cropped automatically based on the xml file. From 400 images, 2,839 single cell images were produced. The crop results are presented in Figure 7 and Figure 8.

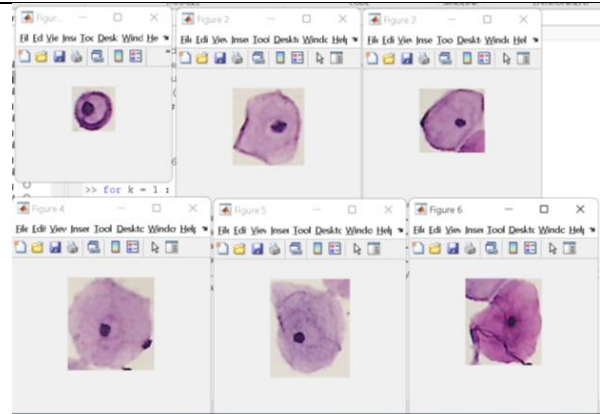


Figure 7. Cropping Results

```
<annotation>
<folder>NA</folder>
<filename>K-CV 1904662-140022 (10).jpg</filename>
<source>
<database>Unknown</database>
</source>
<size>
<width>653</width>
<height>490</height>
<depth>3</depth>
</size>
<segmented>0</segmented>
<object>
<name>Koilocytes</name>
<pose>Unspecified</pose>
<truncated>0</truncated>
<difficult>0</difficult>
<occluded>0</occluded>
<bndbox>
<xmin>169</xmin>
<ymin>29</ymin>
<xmax>253</xmax>
<ymax>115</ymax>
</bndbox>
</object>
<object>
<name>Normal</name>
<pose>Unspecified</pose>
<truncated>0</truncated>
<difficult>0</difficult>
<occluded>0</occluded>
<bndbox>
<xmin>491</xmin>
<ymin>268</ymin>
</bndbox>
</object>
</annotation>
```

Figure 8. Classes and Bounding Boxes from XML files

Each cropped cell is subjected to single cell image nucleus detection in 2 ways, which are presented in Figure 9 and Figure 10.



Figure 9. Image of detection result of Otsu Method

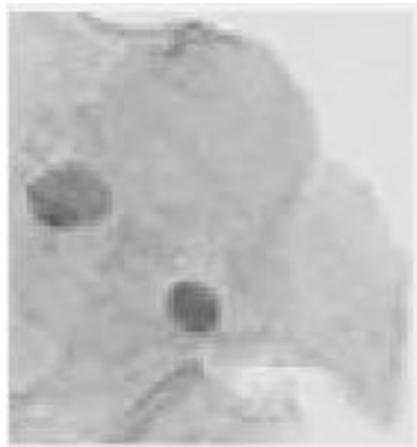


Figure 10. The image resulting from the Polynomial Method detection

The selection of the largest nucleus ROI from each image was processed using GLCM with the default 0-degree angle. The calculation results are presented in Table 1.

Table 1. The GLCM results from Otsu and Polynomial

Method	GLCM Features			
	Contrast	Correlation	Energy	Homogeneity
Otsu	0.1368	0.8983	0.2868	0.9316
Polynomial	0.1410	0.8923	0.2907	0.9300

Table 1 presents the measurement results of various GLCM (Gray-Level Co-occurrence Matrix) features for the Otsu method and the Polynomial method. The following is an interpretation of each GLCM feature:

**Contrast:** This feature measures the extent of intensity differences in the image. Lower values indicate that the image has fewer intensity differences between pixels,

while higher values suggest greater intensity differences. In this case, the Otsu method has a contrast value of 0.1368, while the Polynomial method has a value of 0.1410. The Otsu method has a lower contrast value, indicating fewer intensity differences between pixels in the image.

**Correlation:** This feature measures how pixels in the image are correlated with each other. Values closer to 1 indicate a higher level of correlation between pixels. In this instance, the Otsu method has a correlation value of approximately 0.8983, while the Polynomial method has a value of around 0.8923. The Otsu method has a slightly higher correlation, indicating a higher level of correlation between pixels in the image.

**Energy:** This feature measures the homogeneity or uniformity of intensities in the image. Values approaching 1 indicate that the image has very uniform intensities. In this table, the Otsu method has an energy value of about 0.2868, while the Polynomial method has a value of about 0.2907. The Otsu method has a slightly lower energy value, indicating slightly greater intensity variation in the image.

**Homogeneity:** This feature measures how homogeneous or uniform the intensities in the image are. Values close to 1 indicate that the image is highly homogeneous. In this table, the Otsu method has a homogeneity value of around 0.9316, while the Polynomial method has a value of approximately 0.9300. Both methods exhibit high homogeneity, but the Otsu method has a slight advantage in this regard.

So, the results from this table demonstrate a comparison of various GLCM features between the Otsu and Polynomial methods. The Polynomial method has slightly better values for contrast and energy, but it has a slightly lower correlation and homogeneity value compared to the Otsu method.

The process of calculating the proximity between GLCM features of Otsu and Polynomial methods with reference GLCM features using Euclidean distance is presented in Code 1.

```
[Contrast;Correlation;Energy;Homogeneity];
stats_mat_nor = [0.0594;0.9515;0.4093;0.9738];
stats_mat_LSiL = [0.1750;0.9566;0.1543;0.9147];
stats_mat_HSiL = [0.0339;0.9869;0.2922;0.9831];
stats_mat_koilocyt = [0.2079;0.9726;0.1260;0.9152];
```

The total proximity results for all images from each method are: GLCM Otsu average distance = 6.6457; GLCM Polynomial average distance = 6.6215.

The average distance values for GLCM Otsu and GLCM Polynomial were obtained using the Euclidean distance. The GLCM Otsu value of 6.6457 is larger than the GLCM Polynomial value of 6.6215, indicating that the calculation of Euclidean distance suggests that the

GLCM Polynomial is closer to the reference GLCM value in identifying the nucleus position. This research outcome highlights that smaller Euclidean distance values indicate a closer proximity to the actual nucleus position. The values above represent the overall values for 400 images, which have been averaged. It is evident that the average distance for the polynomial method is closer to the reference GLCM.

### 3.2 Discussions

The practical implications of these findings in the context of cervical cancer diagnosis can be highly beneficial, such as:

**Improved Diagnostic Accuracy:** The superior performance of GLCM Polynomial in nucleus detection has the potential to enhance the accuracy of cervical cancer diagnosis. With more accurate nucleus detection, doctors can have more valuable information for diagnosing cervical cancer at earlier stages, which translates to earlier treatment and improved chances of recovery.

**Reduction of Human Errors:** The enhanced GLCM Polynomial can also help reduce human errors in the diagnostic process. This is because computer algorithms can rely on more reliable and objective data compared to human interpretation, which is susceptible to variations and fatigue.

**Use in Challenging Cases:** The potential application of GLCM Polynomial in diagnostically challenging cases should be considered. There are instances where cervical cancer cells are difficult to distinguish from normal cells with the naked eye. In such situations, advanced computer algorithms can provide significant added value in assisting doctors in making more accurate decisions.

**Limitations in Clinical Application:** However, there are some limitations in the clinical application of GLCM Polynomial. These may include the required hardware and software, computation time, and the training needed for medical professionals to integrate this tool into their daily practice. Additionally, it is important to emphasize that the results of image analysis always need to be confirmed through further medical examinations.

These practical implications highlight the potential benefits of utilizing GLCM Polynomial in cervical cancer diagnosis, while also acknowledging the challenges and limitations that need to be addressed for effective integration into clinical practice.

## 4. Conclusions

This research results in an improvement of the nucleus detection method by integrating the GLCM technique into the Polynomial method. This indicates that the

Polynomial method yields nucleus detections that are, on average, closer to the actual nucleus positions. Considering the superior performance of GLCM Polynomial, further research will apply the performance of this method not only to detect nuclei in single cells but can be extended to detect nuclei within groups of cells. In such cases, nuclei may overlap, posing a unique challenge for precise detection. Furthermore, as part of further research, the GLCM Polynomial method will be validated on external datasets for nucleus detection. A method capable of accurately detecting nuclei can be suggested as a recommendation to improve the method's accuracy in future cervical cancer cell identification.

## Acknowledgments

Applied Research Grant - *Jalur Hilirisasi Kemdikbudristek* 2023 for 3 years (first year) with Contract No: 1426/LL3/AL.04/2023.

## Reference

- [1] D. Riana, M. Jamil, S. Hadianti, J. Na'am, H. Sutanto, and R. Sukwadi, "Model of Watershed Segmentation in Deep Learning Method to Improve Identification of Cervical Cancer at Overlay Cells," *TEM Journal*, pp. 813–819, May 2023, doi: 10.18421/tem122-26
- [2] R. Kavitha et al., "Ant Colony Optimization-Enabled CNN Deep Learning Technique for Accurate Detection of Cervical Cancer," *BioMed Research International*, vol. 2023, pp. 1–9, Feb. 2023, doi: 10.1155/2023/1742891
- [3] G. Duru and S. Topatan, "A barrier to participation in cervical cancer screenings: fatalism," *Women & Health*, vol. 63, no. 6, pp. 436–444, Jun. 2023, doi: 10.1080/03630242.2023.2223698.
- [4] G. Song, J. Han, Y. Zhao, Z. Wang, and H. Du, "A Review on Medical Image Registration as an Optimization Problem," *Current Medical Imaging Reviews*, vol. 13, no. 3, Jul. 2017, doi: 10.2174/1573405612666160920123955.
- [5] J. Bierbrier, H.-E. Gueziri, and D. L. Collins, "Estimating medical image registration error and confidence: A taxonomy and scoping review," *Medical Image Analysis*, vol. 81, p. 102531, Oct. 2022, doi: 10.1016/j.media.2022.102531.
- [6] R. Di Fiore et al., "Cancer Stem Cells and Their Possible Implications in Cervical Cancer: A Short Review," *International Journal of Molecular Sciences*, vol. 23, no. 9, p. 5167, May 2022, doi: 10.3390/ijms23095167.
- [7] D. Riana, A. N. Hidayanto, and Fitriyani, "Integration of Bagging and greedy forward selection on image pap smear classification using Naïve Bayes," 2017 5th International Conference on Cyber and IT Service Management (CITSM), Aug. 2017, doi: 10.1109/citsm.2017.8089320.
- [8] W. Liu et al., "CVM-Cervix: A hybrid cervical Pap-smear image classification framework using CNN, visual transformer and multilayer perceptron," *Pattern Recognition*, vol. 130, p. 108829, Oct. 2022, doi: 10.1016/j.patcog.2022.108829.
- [9] H. L. Glasgow et al., "Laminin targeting of a peripheral nerve-highlighting peptide enables degenerated nerve visualization," *Proceedings of the National Academy of Sciences*, vol. 113, no. 45, pp. 12774–12779, Oct. 2016, doi: 10.1073/pnas.1611642113.
- [10] J. Pulkkinen, H. Huhtala, and I. Kholová, "False-positive atypical endocervical cells in conventional Pap smears: Cytological correlation and analysis," *Acta Cytologica*, Aug. 2023, doi: 10.1159/000533256.

- [11] N. Nahrawi et al., "A review of detection and classification cervical cell images," AIP Conference Proceedings, 2023, doi: 10.1063/5.0127798.
- [12] Nur Ain Alias, Wan Azani Mustafa, Mohd Aminudin Jamlos, Shahrina Ismail, Hiam Alquran, and Mohamad Nur Khairul Hafizi Rohani, "Pap Smear Image Analysis Based on Nucleus Segmentation and Deep Learning – A Recent Review," Journal of Advanced Research in Applied Sciences and Engineering Technology, vol. 29, no. 3, pp. 37–47, Feb. 2023, doi: 10.37934/araset.29.3.3747.
- [13] I. Pacal and S. Kilicarslan, "Deep learning-based approaches for robust classification of cervical cancer," Neural Computing and Applications, vol. 35, no. 25, pp. 18813–18828, Jul. 2023, doi: 10.1007/s00521-023-08757-w.
- [14] W. William, A. Ware, A. H. Basaza-Ejiri, and J. Obungoloch, "A review of image analysis and machine learning techniques for automated cervical cancer screening from pap-smear images," Computer Methods and Programs in Biomedicine, vol. 164, pp. 15–22, Oct. 2018, doi: 10.1016/j.cmpb.2018.05.034.
- [15] Y. Hamama-Raz, S. Shinan-Altman, and I. Levkovich, "The intrapersonal and interpersonal processes of fear of recurrence among cervical cancer survivors: a qualitative study," Supportive Care in Cancer, vol. 30, no. 3, pp. 2671–2678, Nov. 2021, doi: 10.1007/s00520-021-06695-8.
- [16] M. E. Plissiti, P. Dimitrakopoulos, G. Sfikas, C. Nikou, O. Krikoni, and A. Charchanti, "Sipakmed: A New Dataset for Feature and Image Based Classification of Normal and Pathological Cervical Cells in Pap Smear Images," 2018 25th IEEE International Conference on Image Processing (ICIP), Oct. 2018, doi: 10.1109/icip.2018.8451588.
- [17] R. Guido, "Secondary Prevention of Cervical Cancer Part 2," Clinical Obstetrics & Gynecology, vol. 57, no. 2, pp. 292–301, Jun. 2014, doi: 10.1097/grf.0000000000000033.
- [18] I. Rodriguez et al., "Insights into the Mechanisms and Structure of Breakage-Fusion-Bridge Cycles in Cervical Cancer using Long-Read Sequencing," Aug. 2023, doi: 10.1101/2023.08.21.23294276.
- [19] Y. Li, F. Chen, J. Shi, Y. Huang, and M. Wang, "Convolutional Neural Networks for Classifying Cervical Cancer Types Using Histological Images," Journal of Digital Imaging, vol. 36, no. 2, pp. 441–449, Dec. 2022, doi: 10.1007/s10278-022-00722-8.
- [20] F. Kuang, J. Ren, Q. Zhong, F. Liyuan, Y. Huan, and Z. Chen, "The value of apparent diffusion coefficient in the assessment of cervical cancer," European Radiology, vol. 23, no. 4, pp. 1050–1058, Nov. 2012, doi: 10.1007/s00330-012-2681-1.
- [21] J. Jordan et al., "European guidelines for quality assurance in cervical cancer screening: recommendations for clinical management of abnormal cervical cytology, part 1," Cytopathology, vol. 19, no. 6, pp. 342–354, Dec. 2008, doi: 10.1111/j.1365-2303.2008.00623.x.
- [22] H. L. Glasgow et al., "Laminin targeting of a peripheral nerve-highlighting peptide enables degenerated nerve visualization," Proceedings of the National Academy of Sciences, vol. 113, no. 45, pp. 12774–12779, Oct. 2016, doi: 10.1073/pnas.1611642113.
- [23] S. Zhang, Z. Ma, G. Zhang, T. Lei, R. Zhang, and Y. Cui, "Semantic image segmentation with deep convolutional neural networks and quick shift," Symmetry (Basel), vol. 12, no. 3, pp. 1–11, 2020. doi: 10.3390/sym12030427.
- [24] Y. H. Tao Wang, Jinjie Huang, Dequan Zheng, "Nucleus segmentation of cervical cytology images based on depth information," IEE Access, vol. 8, pp. 75846–75859, May 2020, doi: 10.1109/ACCESS.2020.2989369.
- [25] R. Zou et al., "Effects of metalloprotease ADAMTS12 on cervical cancer cell phenotype and its potential mechanism," Discover Oncology, vol. 14, no. 1, Aug. 2023, doi: 10.1007/s12672-023-00776-2.
- [26] J. C. LeCher et al., "Utilization of a cell-penetrating peptide-adaptor for delivery of human papillomavirus protein <sc>E2</sc> into cervical cancer cells to arrest cell growth and promote cell death," Cancer Reports, vol. 6, no. 5, Mar. 2023, doi: 10.1002/cnr2.1810.
- [27] A. Saihood, H. Karshenas, and A. R. Naghsh-Nilchi, "Multi-Orientation Local Texture Features for Guided Attention-Based Fusion in Lung Nodule Classification," IEEE Access, vol. 11, pp. 17555–17568, 2023, doi: 10.1109/access.2023.3243104.
- [28] D. Riana et al., "RepoMedUNM: A New Dataset for Feature Extraction and Training of Deep Learning Network for Classification of Pap Smear Images," in International Conference on Neural Information Processing, 2021, pp. 317–325, doi: 10.1007/978-3-030-92307-5\_37. <https://auth.huaweicloud.com>
- [29] M. Wati, D. Dwiani Samjar, H. Haviluddin, and F. Alameka, "Identifikasi Senjata Tradisional Mandau Suku Dayak Menggunakan Metode Support Vector Machine," Metik J., vol. 6, no. 1, pp. 70–78, 2022, doi: 10.47002/metik.v6i1.341.
- [30] W. Thalib, A. Luhur, and M. W. Paryasto, "Analisis Berat Dan Ukuran Telur Ayam Menggunakan Metode Otsu Berbasis Citra Digital," e-Proceeding Eng., vol. 10, no. 1, pp. 189–195, 2023.
- [31] Hong, G., Luo, M. R., & Rhodes, P. A. "Colorimetric Characterization Based on Polynomial Modeling". Time, 2(Iso 17321), 2000
- [32] N. Merlina, E. Noersasongko, P. N. Andono, M. A. Soeleman, D. Riana, and J. Na, "Medical Image Registration at Pap Smear for Early Identification of Cervical Cancer," TEM J., vol. 12, no. 2, pp. 726–731, 2023, doi: 10.18421/TEM122.
- [33] N. Merlina, E. Noersasongko, P. Nurtantio, M. A. Soeleman, D. Riana, and S. Hadianti, "Detecting the Width of P p S mear Cytoplasm Image Based on GLCM Feature," Y.-D. Zhang et al. (eds.), Smart Trends in Computing and Communications: Proceedings of SmartCom 2020, Smart Innovation, Systems and Technologies 182, [https://doi.org/10.1007/978-981-15-5224-3\\_22](https://doi.org/10.1007/978-981-15-5224-3_22).
- [34] F. Aziz, F. Ernawan, M. Fakhreldin, and P. W. Adi, "YOLO Network-Based for Detection of Rice Leaf Disease," 2023 International Conference on Information Technology Research and Innovation (ICITRI), Aug. 2023, doi: 10.1109/icitri59340.2023.10249843.